Chapter 6
Flood Inundation and Hazard Mapping of 2017 Floods in the Rapti River Basin Using Sentinel-1A Synthetic Aperture Radar Images

Rajesh Kumar

Abstract Globally, the flood magnitude and flood-induced damage are increasing. Hence, the geospatial technology has been used to minimise the adverse effects of floods and to plan the floodplain for the betterment of floodplain dwellers. One of the major causes of floods in the Rapti River basin is heavy rainfall induced by the break-in-monsoon condition. These days, geoscientists and planners use Sentinel-1A IW GRD synthetic-aperture radar (SAR) image for flood extent mapping. Gauge level and flood duration data recorded at Bhinga, Balrampur, Bansi, Regauli, Birdghat, Kakarahi, Uska Bazar and Trimohinighat sites provide the basis for the selection of SAR images. Extensive floods occurred in the Rapti River basin during August 13–September 01, 2017. The flood duration in the Rapti River basin varied from 3 (Bhinga) to 18 days (Birdghat) in 2017. The flood duration, normally, increases from the upstream to downstream along the Rapti River due to decreasing slope and discharges contributed by the tributaries. In this study, Sentinel-1A GRD SAR images of August 21 and 25, 2017, have been selected for flood mapping in the Indian part of the Rapti River basin. The water level of rivers was above the danger level (DL) at Bansi, Regauli, Birdghat, Kakarahi, Uska Bazar and Trimohinighat gauge and discharge (G/D) sites on August 21 and 25, 2017. The propagation of flood peaks and affected areas has been analysed using water level data and SAR images for the mentioned periods. The actual flooded areas covered 2046.7 km^2 area of the Indian part of the Rapti River basin during August 21–25, 2017. The validation of flooded areas has been done using GPS way points collected during field survey (November 2017) and Landsat 7 ETM+ images (August 24, 2017). Breach sites in flood-prone areas have been mapped using Sentinel-2A and B MSI images. The z-score method has been used for the standardisation of development block-wise flooded areas (km^2) and number of flood-affected villages. After standardisation, these two parameters have been added to formulate development

R. Kumar (✉)
Centre for the Study of Regional Development, Jawaharlal Nehru University, New Delhi, India
http://orcid.org/0000-0001-6092-2099

P. Kumar et al. (eds.), *Applications and Challenges of Geospatial Technology*,
https://doi.org/10.1007/978-3-319-99882-4_6

block-wise flood hazard index (FHI). High to very high FHI values have been observed in Siddharthnagar and Gorakhpur districts.

Keywords Sentinel-1A IW GRD SAR · Rapti River basin · Backscatter values · Danger level · Unprecedented flood · Flood hazard index

6.1 Introduction

Earth scientists and planners extensively use satellite images from active and passive remote sensing satellites for quick, accurate and real-time mapping of the flooded areas and hazard assessment in a river basin across the world. Active sensors utilise near-infrared and microwave region of the electromagnetic spectrum for terrestrial mapping (Jensen 2018). These sensors have the capacity to sense the Earth's objects during cloudy and light rainfall weather conditions. These sensors also work round the clock. However, the passive sensors do not detect the Earth's objects at night and during cloudy and light rainfall weather conditions. Hence, satellite images acquired by the active sensor are extensively used for flood mapping and its propagation downstream. But many researchers have used satellite images of the active and passive sensors to map the flood extent, depth, duration and turbidity (Kumar and Acharya 2016; Bhatt et al. 2016; Kumar 2016). Flooded or water pixel extraction from the top-of-atmosphere or surface reflectance images of the passive sensors, namely, Landsat operational land imager and thermal infrared sensor (OLI-TIRS), thematic mapper (TM), enhanced thematic mapper plus (ETM+) and multispectral scanner (MSS), are based on the normalised difference water index (NDWI), modified normalised difference water index (MNDWI), density slicing of near-infrared and shortwave infrared bands, visual interpretation and tasseled cap transformation (Crist and Cicone, 1984; McFeeters 1996; Jain et al. 2006; Xu 2006; Romshoo et al. 2018). Furthermore, the coarse spatial resolution images of Moderate Resolution Imaging Spectroradiometer (MODIS) and National Oceanic and Atmospheric Administration (NOAA) Advanced Very High Resolution Radiometer (AVHRR) sensors are used for large-scale mapping of the flooded areas due to their high temporal resolution (Ahamed and Bolten 2017; Islam and Sado 2000).

Presence of speckles in SAR image is a major disadvantage because it makes the texture analysis of image complicated (Lee 1981). Speckles in SAR images also influence the spatial characteristics of the backscattering coefficient of different Earth's objects that largely depends on surface roughness, dielectric constant, polarisation and incident angle of SAR waves (Senthilnath et al. 2013). Wind-induced ripples, the velocity of floodwaters, heavy rainfall and submerged vegetation and crops make the surface of the flood inundation rough that further creates a problem in image analysis and classification (Huang 2008; Eisuke 2012). Speckle filtering minimises the speckle noise, but it further degrades the resolution and object information of the SAR image (Sheng and Xia 1996; Manavalan 2017). Furthermore, the adaptive speckle filtering methods conserve the edges and texture

information by computing the kernel mean and normalised standard deviation (Senthilnath et al. 2013). Different types of adaptive filters have been developed for the speckle suppression of SAR images. These are mean, median, refined Lee, sigma Lee and Lee (Lee 1981), Frost (Frost et al. 1982) and Gamma MAP (Lopès et al. 1990) filters. According to Qui et al. (2004), "In general, no filter consistently outperforms others. Each filter has its unique strengths and limitations". Hence, the selection of despeckle filter for SAR images depends on the nature of the study (Lee et al. 1994). Manavalan and Rao (2014) pointed out that the despeckle filtering is not necessary when the flood inundation surface is smooth. Flooded area mapping using SAR images is based on different methods like visual interpretation (Oberstadler et al. 1997), Ostu's method and thresholding of backscattering values (Hirose et al. 2001; Yamada 2001; Tan et al. 2004; Bhatt et al. 2013; Manjusree et al. 2015; Ban et al. 2017), band ratio and change detection (Giustarini et al. 2013; Schlaffer et al. 2015), SAR image-based supervised classification (DeRoo et al. 1999; Borghys et al. 2006), fuzzy rules (Pulvirenti et al. 2013), region growing (Mason et al. 2012a; Giustarini et al. 2013) active contour model (ACM) (Kass et al. 1988; Williams and Shah 1992; Horritt 1999), grey-level co-occurrence matrix (GLCM) (Song et al. 2007), segmentation and object-oriented image analysis techniques (Li et al. 2007). Many methods of extracting flooded areas from different SAR images are directly or indirectly based on finding an appropriate threshold range (Manavalan 2017).

Due to improvement in the spatial and temporal resolution, the Sentinel-1A SAR image has been used for detecting floods in rural areas (Clement et al. 2017). However, in urban areas, high density of buildings causes radar shadow and double bouncing effects that further creates a problem in detecting flooded areas (Clement et al. 2017). Therefore, the detection of flooding in urban areas requires fine resolution SAR images of COSMO-SkyMed, TerraSAR-X and RADARSAT-2 (Mason et al. 2012b; Pulvirenti et al. 2016).

In developing countries like India, the flood-prone areas are extensively used for agriculture and business activities. Despite huge investment on flood control measures in India, the flood-induced damage to houses, public utilities, the standing crops and the affected population has been increasing since 1980, inferring encroachment of high-value land use on chronically flood-affected areas (Sivasami 2002). Hence, flood hazard assessment using geospatial technology is a nonstructural measure for minimising the adverse effects of floods in flood-prone areas (Manjusree et al. 2015). Flood hazard assessment in Bihar has been analysed using flood layers (1998–2010), hazard area and number of floods in a year parameters, derived from RADARSAT-1 and RADARSAT-2 (C-band) HH polarisation images (Manjusree et al. 2015).

Uttar Pradesh has the highest flood-prone areas in India. The total flood-prone areas in Uttar Pradesh account for 73,400 km^2 (Planning Commission 2011). However, the total flood-prone areas in the Rapti River basin account for 4322.6 km^2 which is ~5.9% of the total flood-prone areas of Uttar Pradesh. The Rapti River, its tributaries and sub-tributaries experience severe floods in the monsoon season due to heavy downpour. Against the backdrop of above-mentioned methods and studies, the present study aims to map the flooding extent of 2017 floods in the Indian part of

the Rapti River basin and to prepare a flood hazard map at development block level using the parameters, i.e. flooded areas and flood-affected hamlets.

6.2 Study Area

The entire Rapti River basin extends from 26° 18′ 00″ N to 28°33′06″ N and 81°33′00″ E to 83°45′06″ E and accounts for 25,793 km^2 of area, out of which 44% (11,401 km^2) lies in Nepal and 56% (14,392 km^2) in Uttar Pradesh (Fig. 6.1) (Rana et al. 2009; Kumar 2010). Administratively, the Rapti River basin covers Bahraich, Shrawasti, Balrampur, Siddharthnagar, Maharajganj, Gorakhpur, Kushinagar, Deoria, Sant Kabir Nagar and Basti districts of Uttar Pradesh.

The Rapti River originates from the Nepalese part of the lesser Himalaya where this river is known as the West Rapti. It is the largest tributary of Ghaghara River, which, in turn, is a major constituent of the Ganga (Rana et al. 2009; Kumar 2010; Kumar et al. 2013). The Jimruk, *Burhi* Rapti and its tributaries, Rohini and Gaura River are the major left bank tributaries of the Rapti. The right bank tributaries are Ami and Taraina River. In the Indian part of the basin, six gauge and discharge (G/D) sites, namely, Kakardhari, Bhinga, Balrampur, Bansi, Regauli and Birdghat (Gorakhpur), are located along the Rapti River. Kakarahi, Uska Bazar and

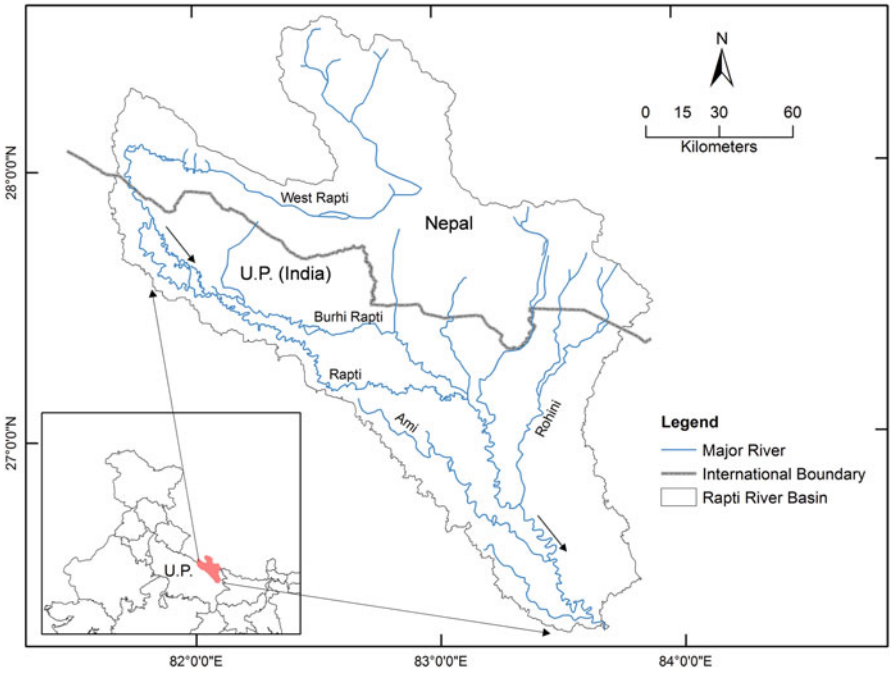

Fig. 6.1 Location map of the study area

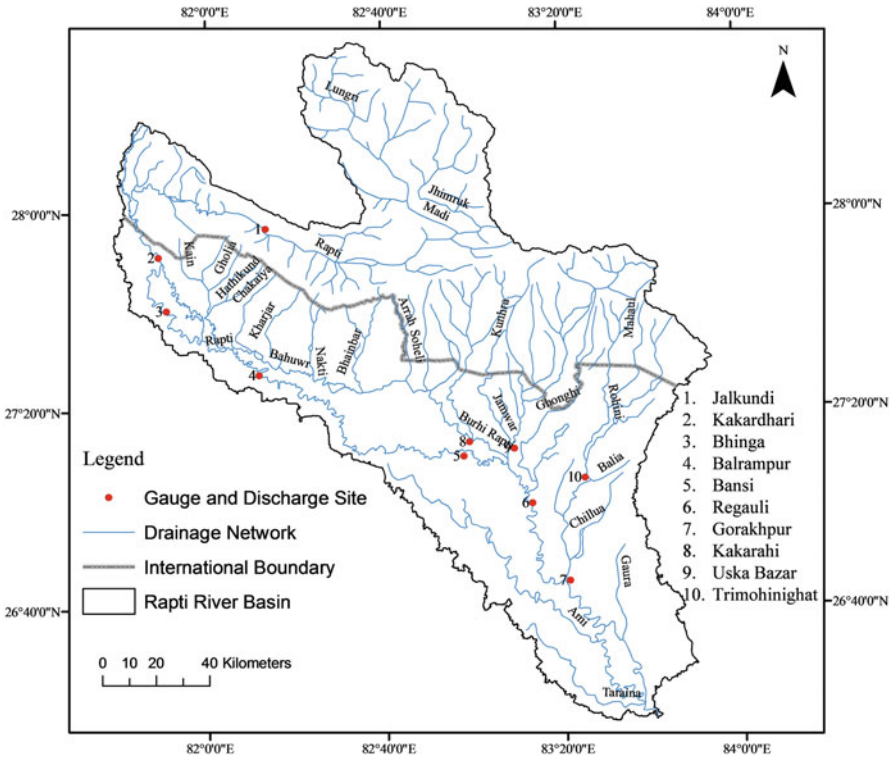

Fig. 6.2 Drainage map and gauge and discharge (G/D) sites of the Rapti River basin

Trimohinighat G/D sites are located along the *Burhi* Rapti, Kunhra and Rohini River, respectively (Fig. 6.2). The study region is a part of the vast alluvial plain of the Ganga where the depth of alluvium varies from ~4 to 6 km (Singh 1996). The major geomorphic features of the study area are piedmont alluvial plain, older alluvial plain, older floodplain and active floodplain (GSI and NRSC 2012). Furthermore, the active and older floodplains constitute the flood-prone areas of the Rapti River basin. In this study, areas bordered by the embankments are mapped as an active floodplain. The older floodplain is protected by the embankments. However, breaches in embankments cause flooding therein (Fig. 6.3). Agriculture is a general land use pattern in the study area (Yadav 1999).

6.3 Material and Methodology

Sentinel-1 consists of two-satellite constellation, namely, Sentinel-1A and Sentinel-1B. Sentinel-1A C-band SAR operated at a frequency of 5.405 GHz to detect the Earth's objects. Sentinel-1A and B missions were launched on April 3, 2014, and

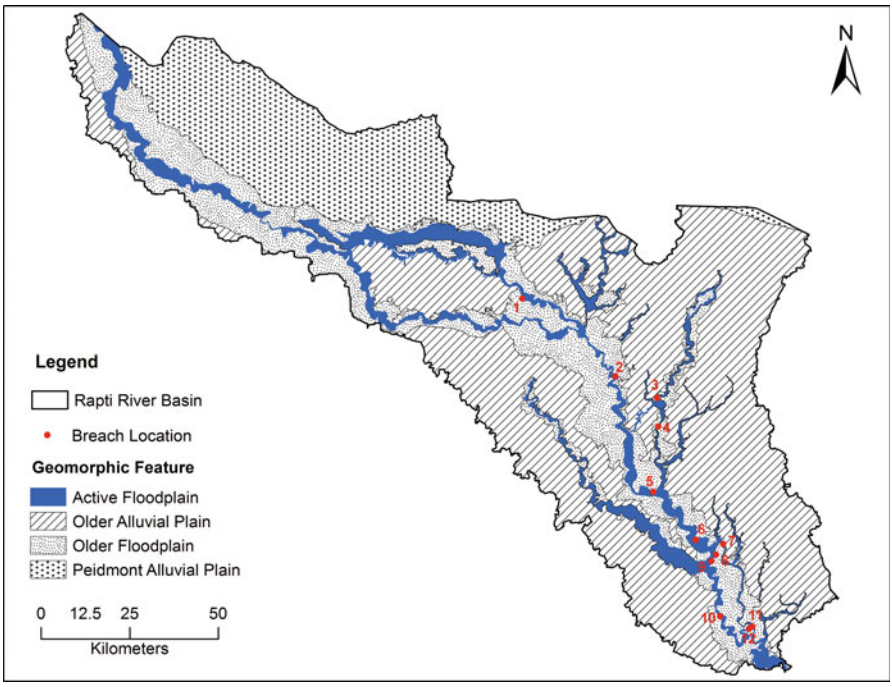

Fig. 6.3 Geomorphic features of the study area along with breach locations due to 2017 floods (Modified after GSI and NRSC 2012)

April 25, 2016, by the European Space Agency (ESA) under Europe's Copernicus programme, respectively, (ESA 2018a). The orbit height of Sentinel-1A and B is 693 km with a combined temporal resolution of 6 days. However, the temporal resolution of a single Sentinel-1 satellite is 12 days at the equator (ESA 2018a). The level-1 ground range detected (GRD) data products of Sentinel-1A have been used in this study. Interferometric wide swath (IW) GRD data product has dual polarisation modes, i.e. VV and VH. With the help of an Earth ellipsoid model, the GRD level-1 data have been detected, multi-looked and projected to the ground range (ESA 2018b). Sentinel-2 is a multispectral instrument (MSI). This is a two-satellite constellation, namely, Sentinel-2A and Sentinel-2B that were launched on June 23, 2015, and March 07, 2017, by the ESA, respectively (ESA 2018c). The temporal resolution of the combined Sentinel-2 satellites is 5 days at the equator, while it is 10 days for a single satellite (ESA 2018c). The height of the orbit of Sentinel-2A and B satellite is at 786 km (ESA 2018c). Sentinel-2 operates in visible, near-infrared and shortwave infrared part of the electromagnetic spectrum (Table 6.1) (ESA 2018d).

The Sentinel-1A SAR images have been used for mapping the flooded areas and pre-flood water bodies, while the Sentinel-2 images have been used for mapping of

Table 6.1 Spectral bands of the Sentinel-2A and B sensor

Band number	Band name	Sentinel-2A		Sentinel-2B		
		Central wavelength (nm)	Bandwidth (nm)	Central wavelength (nm)	Bandwidth (nm)	Spatial resolution (m)
1	Coastal aerosol	443.9	27	442.3	45	60
2	Blue	496.6	98	492.1	98	10
3	Green	560	45	559	46	10
4	Red	664.5	38	665	39	10
5	Vegetation red edge	703.9	19	703.8	20	20
6	Vegetation red edge	740.2	18	739.1	18	20
7	Vegetation red edge	782.5	28	779.7	28	20
8	NIR	835.1	145	833	133	10
8a	Vegetation red edge	864.8	33	864	32	20
9	Water vapour	945	26	943.2	27	60
10	Cirrus	1373.5	75	1376.9	76	60
11	SWIR	1613.7	143	1610.4	141	20
12	SWIR	2202.4	242	2185.7	238	20

Source: Sentinel online (2018)

the geomorphic features and breach sites. Landsat 7 ETM+ images of 30 m spatial resolution (EarthExplorer 2017) have been used for accuracy assessment of flooded and non-flooded areas extracted from the Sentinel-1 SAR images (Table 6.2). The Shuttle Radar Topography Mission (SRTM) digital elevation model (DEM) at 90 m spatial resolution (CGIAR-CSI 2008) has been used to extract the Rapti River basin boundary using hydrology module of the spatial analyst tool of ArcGIS 10. The development block boundaries have been digitised from the administrative atlas of Uttar Pradesh (Census of India 2001). The hamlet point feature data have been obtained from Mizushima Laboratory (2013). The geomorphic map has been obtained from Bhuvan, an Indian Geo-platform of ISRO (GSI and NRSC 2012). The rainfall and water level data have been obtained from the irrigation department of Uttar Pradesh (Irrigation & Water Resource Department 2017). Synoptic weather system information has been collected from all India weekly weather report (August 10–15, 2017), India Meteorological Department (IMD), Govt. of India (IMD 2017).

In this study, the Sentinel-1A IW GRD products of VV and VH polarisations have been processed using Sentinel Application Platform (SNAP) tool. The pre-processing steps using SNAP tool are given in Fig. 6.4. The standard procedures such as orbit correction, thermal noise removal, calibration (sigma0), speckle

Table 6.2 Description of satellite images

Scene ID	Date of acquisition	Track	Orbit
Sentinel-1A SAR scene IDs and location			
S1A_IW_GRDH_1SDV_20170602T122944_20170602T123009_016855_01C070_F427 (Naugarh-Regauli-Gorakhpur-Barhalganj)	June 02, 2017	158	16,855
S1A_IW_GRDH_1SDV_20170610T002751_20170610T002816_016964_01C3DB_561F ((Bansi-Regauli-Gorakhpur)	June 10, 2017	92	16,964
S1A_IW_GRDH_1SDV_20170610T002726_20170610T002751_016964_01C3DB_B609 (Kakardhari-Balrampur-Bansi)	June 10, 2017	92	16,964
S1A_IW_GRDH_1SDV_20170821T002730_20170821T002755_018014_01E3D1_6DE6 (Kakardhari-Balrampur-Bansi)	August 21, 2017	92	18,014
S1A_IW_GRDH_1SDV_20170821T002755_20170821T002820_018014_01E3D1_FABE (Bansi-Regauli-Gorakhpur)	August 21, 2017	92	18,014
S1A_IW_GRDH_1SDV_20170825T122949_20170825T123014_018080_01E5C1_50D7 (Naugarh-Regauli-Gorakhpur-Barhalganj)	August 25, 2017	158	18,080
Sentinel-2A and B (MSI)			
S2B_MSIL2A_20171016T050749_N0205_R019_T44RPR_20171016T051820.SAFE	October 12, 2017	N.A.	N.A.
S2B_MSIL2A_20171023T045829_N0206_R119_T44RQQ_20171023T084707.SAFE	October 23, 2017	N.A.	N.A.
S2A_MSIL2A_20171028T045911_N0206_R119_T44RQR_20171028T084742.SAFE	October 28, 2017	N.A.	N.A.
Landsat 7 ETM+		Path	Row
LE07_L1GT_142041_20170824_20170824_01_RT	August 24, 2017	142	41
LE07_L1TP_142042_20170824_20170824_01_RT	August 24, 2017	142	42

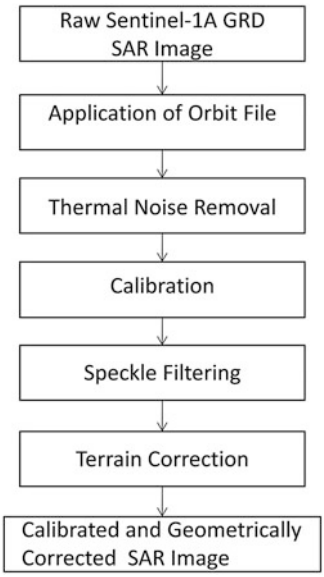

Fig. 6.4 Pre-processing steps of Sentinel-1A GRD SAR image

filtering and terrain correction have been applied on the raw SAR images to obtain the geometrically correct image along with backscattering values (sigma0) (Twele et al. 2016; Clement et al. 2017). A 7 × 7 Gamma MAP filtering method has been used for speckle suppression of the Sentinel-1A GRD SAR images. The sigma0 values have been converted into logarithmic scale, i.e. decibel (dB).

In this study, the selection of SAR images is based on the flood occurrence, duration and movement of the flood crest downstream. The statistics of training sites of flooded areas computed from VV and VH polarisation images of August 21, 2017 show unimodal distribution. Hence, the VV polarisation images of August 21, 2017 have been used for flood pixel extraction. Many researchers concluded that the VV polarisation of Sentinel-1A IW GRD product is appropriate for the flood detection (Twele et al. 2016). But VV polarisation is more affected by wind-induced ripples on the surface of the floodwaters than other polarisations (Manjusree et al. 2012). The VH polarisation image of August 25, 2017 provides better results for mapping the flooded areas than the VV polarisation using thresholding of the backscattered values. The histogram of training site statistics of the VV polarisation image of August 25, 2017, shows a polymodal distribution, while it is a unimodal distribution for VH polarisation image (Fig. 6.5). Hence, the computation of threshold value for the extraction of flooded areas from VH polarisation image is easy and appropriate.

After pre-processing, a thresholding procedure has been used to extract the flood pixels from the Sentinel-1A IW GRD SAR images. On the basis of statistics of the training sites of the flooded areas (minimum, mean, median and standard deviation),

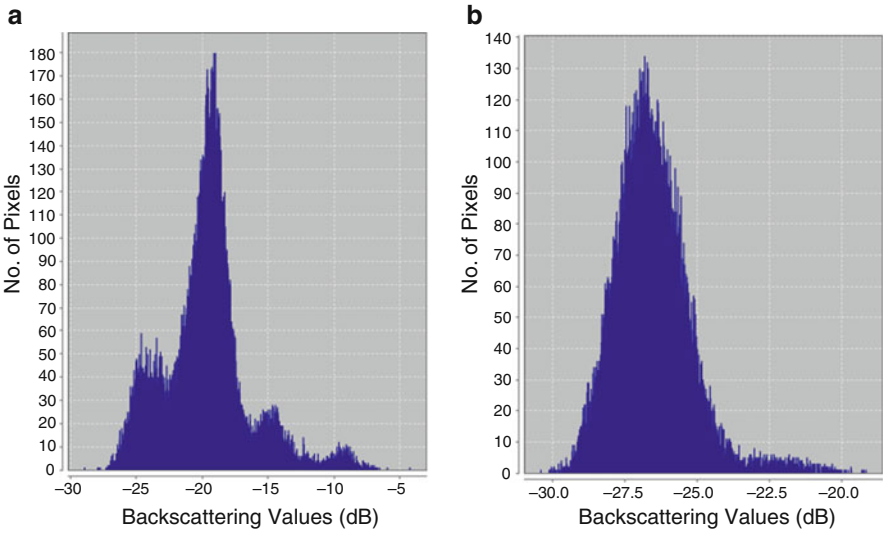

Fig. 6.5 Histogram of backscattering values (dB) of training sites of flooded areas (**a**) VV polarization and (**b**) VH polarisation of Sentinel-1A IW GRD SAR image (August 25, 2017)

lower and upper limit of the threshold range has been decided. Backscattering values (dB) of the flood areas are normally distributed for which the mean ± 3 standard deviation covers 99.7% of the distribution (Fig. 6.5) (Motulsky 2014). In this study, the lowest value of all training sites has been taken as the lower limit of the threshold range. The upper limit (UL) has been obtained using Eq. (6.1):

$$UL = [(\mu + 3\sigma)] \tag{6.1}$$

where σ stands for the standard deviation of training site backscattered values in decibel (dB) and μ is the mean backscattering values of training sites (flooded areas).

The actual flooded areas have been obtained by subtracting the pre-flood water bodies (June 02–10, 2017) from the total flooded areas of August 21–25, 2017. The accuracy assessment of actual flooded and non-flooded areas of August 25, 2017 has been done with the help of the Garmin eTrex global positioning system (GPS) waypoints and reference points selected from the Landsat 7 ETM+ images (August 24, 2017). The overall accuracy of flooded and non-flooded areas of August 25, 2017 is 91.6% with a high kappa coefficient value of 0.83. The user's accuracy for the flooded areas is 94.87% (Table 6.3).

The breach sites in the embankments have been mapped through visual interpretation of false colour composite (FCC) of Sentinel-2 MSI post-flood images (10 m spatial resolution). The development block-wise flood hazard assessment of 2017

Table 6.3 Accuracy assessment of flooded and non-flooded areas (August 25, 2017)

Class	Producer accuracy (%)	User accuracy (%)	Producer accuracy (pixels)	User accuracy (pixels)
Flooded Areas	88.1	94.87	37/42	37/39
Non-flooded areas	95.12	88.64	39/41	39/44

Overall accuracy, (76/83), 91.6% Kappa coefficient, 0.83

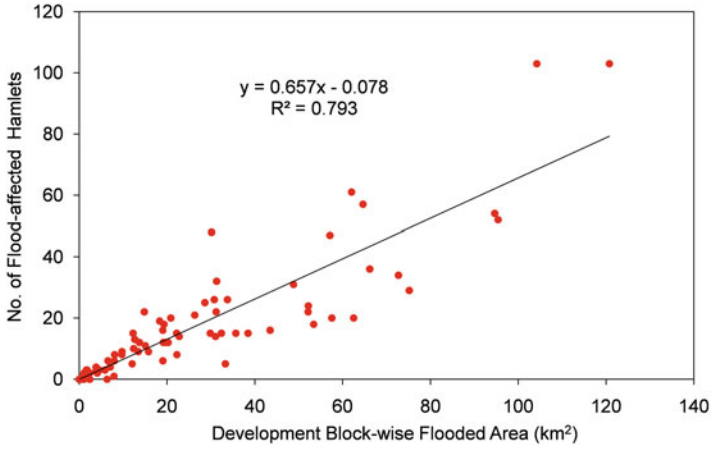

Fig. 6.6 Association between development block-wise flooded areas and flood-affected hamlets

floods has been based on two parameters, namely, development block-wise flooded areas and number of flood-affected hamlets. The linear association between these two parameters is strongly positive as the coefficient of determination (R^2) value is 0.79 (Fig. 6.6). Hence, the z-score (z) method has been applied for the standardisation of these two parameters (Eq.6.2) (Burt et al. 2009):

$$z = (\chi - \mu)/\sigma \tag{6.2}$$

where χ stands for a parameter. μ and σ are mean and standard deviation of a parameter, respectively.

The z-score values of these two parameters have been added linearly to make a composite index, i.e. flood hazard index (FHI). Furthermore, the development block-wise FHI values have been classified into four categories using natural break classification method.

6.4 Results and Discussion

6.4.1 Cause and Occurrence of 2017 Floods

The 2017 floods in the Rapti River basin were caused by the heavy rainfall during August 12–14 due to the break-in-monsoon system (IMD 2017). The highest rainfall of 303.6 mm was recorded at Kakarahi G/D site on August 14. Overall, the high rainfall was recorded at all the G/D sites of the basin on August 14 (Fig. 6.7). Hence, flooding was observed at all the G/D sites except Kakardhari. The flood peak which occurred at Bhinga on August 14 takes 2 days to reach Balrampur G/D site. The synchronisation of peak floods occurred at Bansi, Regauli and Birdghat. The unprecedented flood occurred at Bansi on August 21, 2017, when the water level crossed the previous highest flood level (1998) by 0.06 m. The flood peaks at Trimohinighat, Kakarahi and Uska Bazar occurred on August 16, 18 and 20, 2017, respectively. Deviation of the maximum water level (MWL) from the danger level (DL) at Bansi, Regauli, Birdhat, Kakarahi, Trimohinighat and Uska Bazar was large and ranged between 1.53 and 3.14 m. Such a large deviation of MWL indicates that the major floods occurred at these G/D sites in 2017 (Table 6.4). When the water level in a river remains above the DL by 1 m or more, it is defined as major floods (Dhar and Nandargi 2003).

The flood duration in the basin varied from 3 (Bhinga) to 18 days (Birdghat) during 2017 floods. The flood duration along the Rapti River in the basin showed an increasing trend from upstream to downstream due to decrease in slope and discharges contributed by the tributaries. Hence, the extreme downstream Birdghat G/D site recorded the highest flood duration of 18 days from August 15 to September 01, 2017 (Table 6.5).

Due to the high water level in Rapti, Burhi Rapti, Gaura and Rohini River, breaches in embankments occurred during 2017 floods. A breach of 130 m length occurred in the right embankment of the Burhi Rapti River (breach ID 1) (Table 6.6).

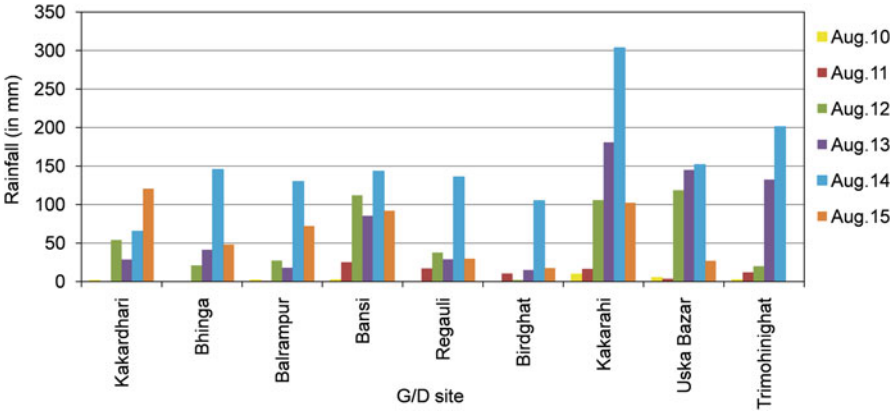

Fig. 6.7 Rainfall recorded at different G/D sites during August 10–15, 2017

Table 6.4 Maximum water level (MWL), danger level (DL) and highest flood level (HFL) in Rapti River basin

G/D Site	DL (m)	MWL, 2017 (m)	Date	Deviation of MWL from DL (m)	HFL (year)
Kakardhari	131	130.77	August 13, 2017	−0.23	132.37 (2014)
Bhinga	119.5	120.11	August 14, 2017	0.61	120.3 (2014)
Balrampur	104.62	105.52	August 16, 2017	0.90	105.51 (2014)
Bansi	84.9	85.88	August 21, 2017	0.98	85.82 (1998)
Regauli	80.3	81.84	August 21, 2017	1.54	82.12 (2000)
Birdghat	74.98	77.22	August 21, 2017	2.24	77.54 (1998)
Kakarahi	85.65	88.79	August 18, 2017	3.14	88.97 (1998)
Uska Bazar	83.52	85.05	August 20, 2017	1.53	85.62 (1998)
Trimohinighat	82.44	85.23	August 16, 2017	2.79	85.43 (2001)

Source: Irrigation and Water Resource Department (2017)

Table 6.5 Flood duration in Rapti River basin during 2017

G/D site	River	Days above DL	Date
Kakardhari	Rapti	0	N.A.
Bhinga	Rapti	3	August 13–15
Balrampur	Rapti	8	August 13–20
Bansi	Rapti	11	August 16–26
Regauli	Rapti	15	August 15–29
Birdghat	Rapti	18	August 15–September 01
Kakarahi	Burhi Rapti	14	August 14–27
Uska Bazar	Kunhra	12	August 15–26
Trimohinighat	Rohini	11	August 13–23

Source: Irrigation and Water Resource Department (2017)

Two breach sites (ID 3 & 4) were located along the Rohini River (Fig. 6.3). Two breaches (ID 7 & 11) were also mapped along the right bank embankment of the Gaura River. The rest of the breach sites were located along the Rapti River. The largest breach (ID 9) of 132 m occurred in the left bank embankment of the Rapti River. Such large breaches in embankments indicate that the structural measure is not a permanent solution for flood control in the basin. Breaches in embankment often produce more coarse to medium sand in the floodwaters that settle in the nearby embankment-protected arable land. Such deposition of coarse and medium sand in the arable land makes it infertile for many years (Kumar 2010).

Table 6.6 Breach in embankments during 2017 floods

Breach site ID	River name	Length (m)
1	Burhi Rapti	130
2	Rapti	40
3	Rohini	50
4	Rohini	80
5	Rapti	110
6	Rapti	36
7	Gaura	99.3
8	Rapti	71.9
9	Rapti	132
10	Rapti	23.9
11	Gaura	113
12	Rapti	94.4

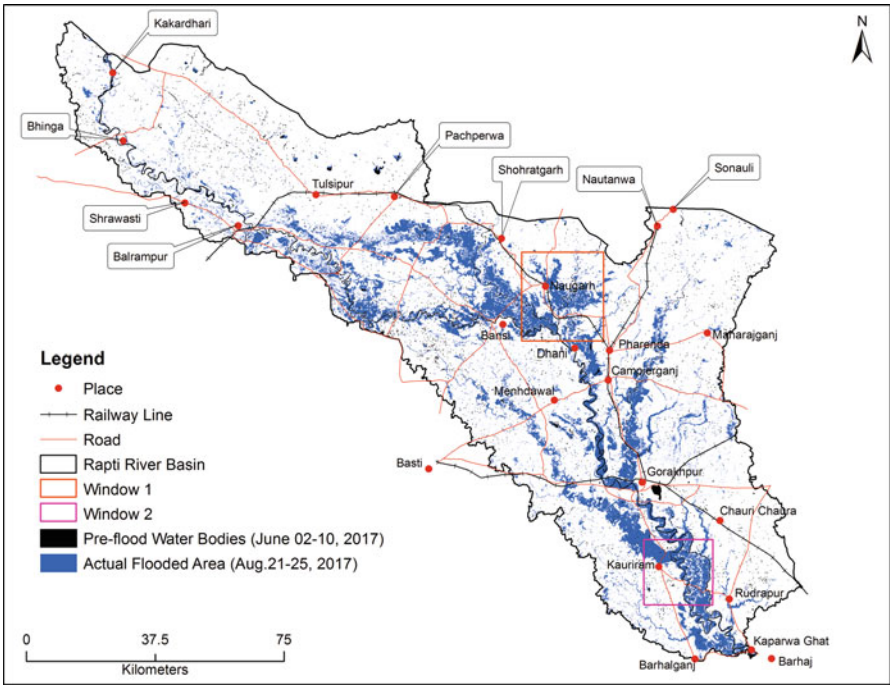

Fig. 6.8 Actual flooded areas and pre-flood water bodies of the Rapti River basin (Indian part)

6.4.2 Flooded Area of the Rapti River Basin in 2017

The actual flooded area in the basin is 2046.7 km^2, while the pre-flood water bodies account for 68.6 km^2 only (Fig. 6.8). The flood-prone area covers 30% geographical area of the Rapti River basin (UP). During 2017 floods, the actual flooded areas

account for 38.8% geographical area of the total flood-prone area. The actual flooded areas of the flood-prone region cover 80% of the total actual flooded areas of the basin.

6.4.3 Downstream Movement of 2017 Floods

Downstream movement of the flood has been analysed with the help of flood extent in window 1 and window 2. The actual flooded area in window 1 on August 21, 2017, was 205 km^2, while it was 131 km^2 on August 25, 2017 (Fig. 6.9). The water level recorded at Kakarahi and Uska Bazar G/D site was above the DL with a decreasing trend during August 21–25, 2017 (Table 6.7). The window 2 largely covers the older floodplain between the Rapti and Gaura River downstream of Birdghat G/D site. The actual flooded area in window 2 was 91 km^2 on August 21, 2017, while it was increased to 143 km^2 on August 25, 2017 (Fig. 6.10). The main causal factor for an increase in flooded area was breaches in embankments along the Rapti and Gaura River. Such breaches in the embankments in window 2 were caused by the flood flow from the upstream reaches.

6.4.4 Development Block-Wise Flood Hazard Assessment

Flood hazard assessment in a populated river basin is basically based on certain key parameters such as elevation, flooded areas, turbidity, flood frequency, depth,

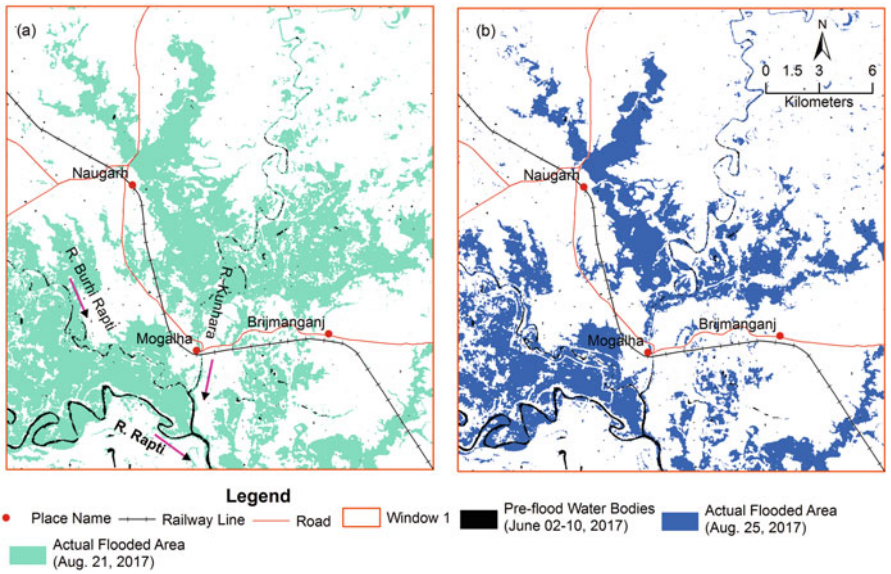

Fig. 6.9 (**a**) and (**b**) Actual flooded areas on August 21 and 25, 2017 in the window 1

Table 6.7 Danger level (DL), water level (WL) and deviation of WL from DL in Rapti River basin during August 21 and 25, 2017

G/D Site	Danger level (m)	WL (August 21, 2017) (m)	WL (August 25, 2017) (m)	Deviation of WL from DL (m) (August 21, 2017)	Deviation of WL from DL (m) (August 25, 2017)
Kakardhari	131	129.01	128.83	−1.99	−2.17
Bhinga	119.5	118.06	118.11	−1.44	−1.39
Balrampur	104.62	104.51	103.98	−0.11	−0.64
Bansi	84.9	85.88	85.33	0.98	0.43
Regauli	80.3	81.84	81.4	1.54	1.1
Birdghat	74.98	77.22	76.6	2.24	1.62
Kakarahi	85.65	87.71	86.93	2.06	1.28
Uska Bazar	83.52	84.99	84.09	1.47	0.57
Trimohinighat	82.44	83.92	81.63	1.48	−0.81

Source: Irrigation and Water Resource Department (2017)

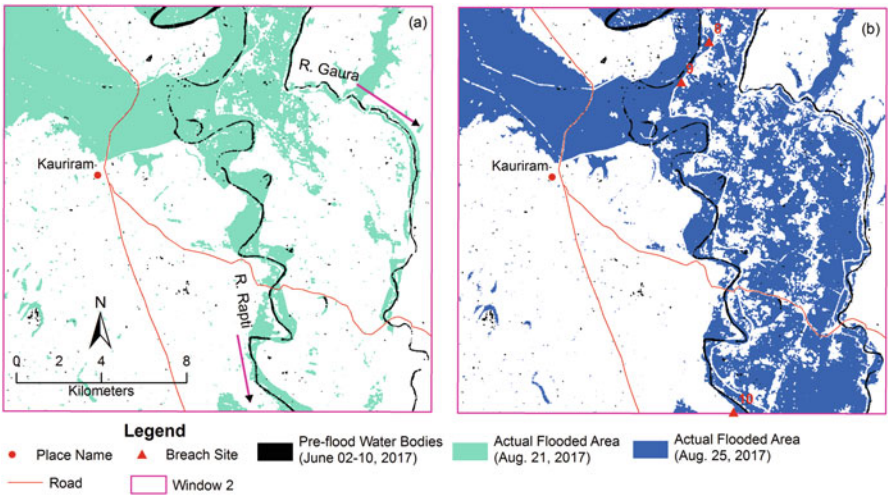

Fig. 6.10 (**a**) and (**b**) Actual flooded areas on August 21 and 25, 2017 in the window 2 along with breach locations

duration, flood-affected population and hamlets (Sanyal and Lu 2006; Manjusree et al. 2015; Kumar and Acharya 2016; Kumar 2016; Kumar et al. 2016). In this study, the development block-wise flooded areas show the extent of flooding, while the number of flood-affected hamlets indicates the flood-induced damage. Therefore, a composite index (FHI) has been computed using these parameters.

In this study, development block-wise low flood hazard is observed in all districts except Siddharthnagar (Fig. 6.11). Generally, the low flood hazard zone

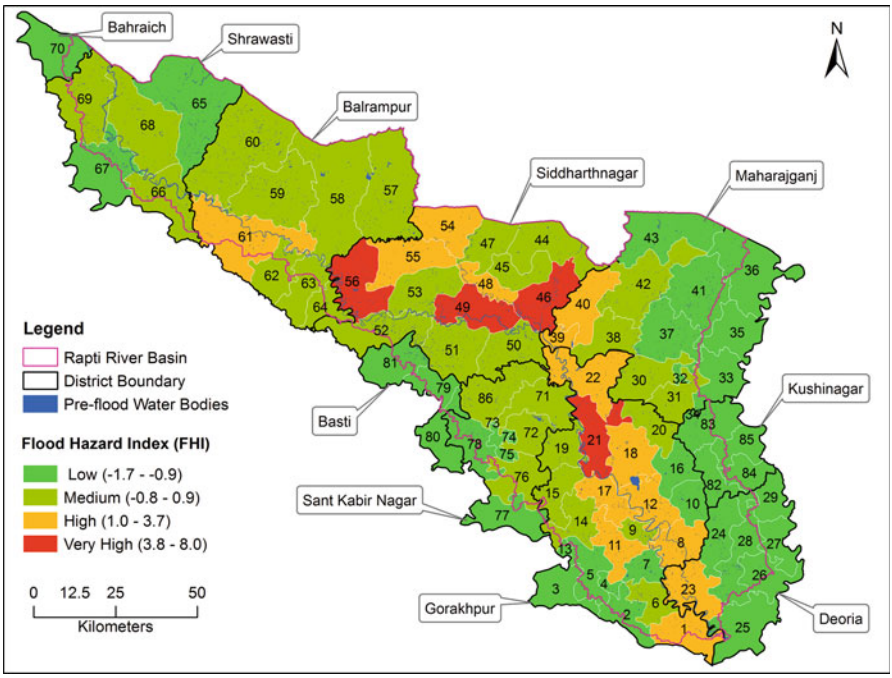

Fig. 6.11 Development block-wise flood hazard categories with label IDs. Name of the districts is given in callouts

Table 6.8a District-wise flood-affected development blocks in low flood hazard zone

District	Affected development block (label ID)
Bahraich	Nawabganj (70)
Shrawasti	Sirasia (65) and Gilaula (67)
Maharajganj	Part of Siswa Bazar (32), Ghughuli (33), part of Partawal (34), Siswa Bazar (35), Nichlaul (36), Maharajganj (37), Mithaura (41) and Nautanwa (43),
Kushinagar	Sukrauli (82), Captanganj (83), Hata (84) and Motichak (85)
Deoria	Gauri Bazar (24), Barhaj (25), Deoria (26), Rampur Karkhana (27), Baitalpur (28) and Desai Deoria (29)
Gorakhpur	Gola (2), Belghat (3), part of Gagaha (4), Urua (5), part of Kauriram (7) and part of Belghat (13)
Sant Kabir Nagar	Part of Semariyawan (73, 74 & 78) and Baghauli (75)
Basti	Rudhauli (79), Saughat (80) and Ramnagar (81)

lies in the older alluvial plain that comes under flood-free zone or *Bangar* land (Table 6.8a).

Medium flood hazard zone is found in the development blocks of Shrawasti, Balrampur, Siddharthnagr, Maharajganj, Gorakhpur and Sant Kabir Nagar districts

Table 6.8b District-wise flood-affected development blocks in medium flood hazard zone

District	Affected development block (Label ID)
Shrawasti	Ikauna (66), Hariharpur (68) and Jamunaha (69)
Balrampur	Pachperwa (57), Gainsari (58), Tulasipur (59), Harraiya Satgharwa (60), Shridattganj (62), Utraula (63) and Gaindas Buzurg (64)
Siddharthnagar	Birdpur (44), Naugarh (45), Shohratgarh (47), Kheserha (50), Mithwal (51) and Domariyaganj (52)
Maharajganj	Paniara (30), Partawal (31), Pharenda (38) and Lakshmipur (42)
Gorakhpur	Gagaha (6), Kauriram (9), Khajani (14), Shahjanwa (15) and Pali (19)
Sant Kabir Nagar	Mehdawal (71), Semariyawan (72), Khalilabad (76) and Santha (86)

Table 6.8c District-wise flood-affected development blocks in high flood hazard zone

District	Affected development block (Label ID)
Balrampur	Balrampur (61)
Siddharthnagar	Jogiya Khas (48), Barhni Bazar (54) and Itwa (55)
Maharajganj	Dhani (39) and Brimanganj (40)
Deoria	Rudrapur (23)
Gorakhpur	Barhalganj (1), Brahmpur (8), Bansgaon (11), Khorabar (12), Piprauli (17), Chargawan (18) and Campierganj (22)

Table 6.8d District-wise flood-affected development blocks in very high flood hazard zone

District	Affected development block (Label ID)
Siddharthnagar	Uska Bazar (46), Bansi (49) and Bhanwapur (56)
Gorakhpur	Jungal Kaudia (21)

(Table 6.8b). In general, this flood zone falls in the topographically low-lying areas of older alluvial plain and older floodplain. Such low-lying areas comprise oxbow lakes, abandoned and minor channels. In the local language, these lakes and channels are called as *chaurs* that often get flooded during the monsoon season. The high flood hazard zone falls in the development blocks of Balrampur, Siddharthnagar, Maharajganj, Deoria and Gorakhpur districts (Table 6.8c). This zone covers the topographically low-lying areas of older alluvial plain, older and active floodplain.

In Siddharthnagar district, a very high flood zone is observed in Uska Bazar, Bansi and Bhanwapur development blocks that fall in the active floodplain of Kunhra, Rapti and Burhi Rapti River (Fig. 6.11). Jungle Kaudia development block of Gorakhpur district also falls in the very high flood zone (Table 6.8d). Jungle Kaudia block comes under the older and active floodplain of Rapti and Rohini River. The topographically low-lying areas of the older floodplain of this block are protected by embankments. Breaches in embankments along the Rohini and Rapti Rivers often cause floods in Jungle Kaudia block.

6.5 Conclusions

The 2017 floods in the Rapti River basin have been caused by the heavy rainfall due to the break-in-monsoon condition. Breaches in embankments are another reason for flooding in embankment-protected areas, i.e. older floodplain. Major floods occurred at Regauli, Birdghat, Kakarahi, Uska Bazar and Trimohinighat G/D sites in 2017.

Siddharthnagar and Gorakhpur were the most flood-affected districts in 2017. The confluence of the *Burhi* Rapti and Rohini River with the Rapti comes under the very high flood hazard zone due to backwater effect. The development block-wise flood hazard zone of a major flood in the Rapti River basin has immense importance to the district administration for the execution of flood management strategies at the block level. The geospatial approach used in this study for flood hazard assessment can be improved with the help of amount of compensation money given to the floodplain dwellers whose houses were damaged by the 2017 floods.

Methods discussed in this study are easy to detect flood-affected areas during the monsoon season using freely available Sentinel-1A IW GRD SAR images. Sentinel-1A SAR detects the Earth's objects round the clock and during cloudy and light rainfall weather conditions. Hence, Sentinel-1 GRD SAR images have immense potential for the implementation of flood fighting measures during floods.

Acknowledgements The author thankfully acknowledges the IMD and Irrigation and Water Resource Department of Uttar Pradesh for providing synoptic weather condition, daily rainfall and water level data of 2017 free of cost. He also expresses gratitude to ESA Copernicus Open Access Hub and USGS EarthExplorer web portals for providing free access to the Sentinel-1A GRD and Landsat 7 ETM+ images, respectively. He also acknowledges ESA science toolbox exploitation platform for providing SNAP tool (ver.6.0.0).

References

Ahamed A, Bolten JD (2017) A MODIS-based automated flood monitoring system for southeast asia. Int J Appl Earth Obs Geoinf 61:104–117. https://doi.org/10.1016/j.jag.2017.05.006

Ban HJ, Kwon YJ, Shin H, Ryu HS, Hong S (2017) Flood monitoring using satellite-based RGB composite imagery and refractive index retrieval in visible and near-infrared bands. Remote Sens. https://doi.org/10.3390/rs9040313

Bhatt CM, Rao GS, Begum A, Manjusree P, Sharma SVSP, Prasanna L, Bhanumurthy V (2013) Satellite images for extraction of flood disaster footprints and assessing the disaster impact: Brahmaputra floods of June–July 2012, Assam, India. Curr Sci 104(12):1692–1700

Bhatt CM, Rao GS, Farooq M, Manjusree P, Shukla A, Sharma SVSP, Kulkarni SS, Begum A, Bhanumurthy V, Diwakar PG, Dadhwal VK (2016) Satellite based assessment of the catastrophic Jhelum floods of September 2014, Jammu & Kashmir, India. Geomat Nat Haz Risk. https://doi.org/10.1080/19475705.2016.1218943

Borghys D, Yvinec Y, Perneel C, Pizurica A, Philips W (2006) Supervised feature-based classification of multi-channel SAR images. Pattern Recogn Lett 27(4):252–258

Burt JE, Barber GM, Rigby DL (2009) Elementary statistics for geographers, 3rd edn. The Guilford Press, New York

Census of India (2001) Administrative atlas of Uttar Pradesh. Office of the Registrar General & Census Commissioner, New Delhi

CGIAR-CSI (2008) SRTM 90m digital elevation data. http://srtm.csi.cgiar.org/SELECTION/inputCoord.asp. Accessed on 01 Jan 2008

Clement MA, Kilsby CG, Moore P (2017) Multi-temporal synthetic aperture radar flood mapping using change detection. J Flood Risk Manage. https://doi.org/10.1111/jfr3.12303

Crist EP, Cicone RC (1984) A physically-based transformation of thematic mapper data—the TM tasseled cap. IEEE Trans Geosci Remote Sens 22:256–263. https://doi.org/10.1109/TGRS.1984.350619

De Roo A, Van der Knijff J, Horritt MS, Schmuck G, De Jong S (1999) Assessing flood damages of the 1997 Oder flood and the 1995 Meuse flood. Proceedings of the 2nd international symposium on operationalisation of remote sensing, Enschede, The Netherlands, pp 3459–3465

Dhar ON, Nandargi S (2003) Hydrometeorological aspects of floods in India. Nat Hazards 28:1–33

EarthExplorer (2017) Landsat collection 1 level-1, Landsat7 ETM+ C1 level-1. https://earthexplorer.usgs.gov/. Accessed on 30 Aug 2018

Eisuke K (2012) Basic principles of Synthetic Aperture Radar (SAR). 8th Sentinel Asia System (SAS) Operation Training, Bangkok

ESA (2018a) Sentinel-1 mission details. https://earth.esa.int/web/guest/missions/esa-operational-eo-missions/sentinel-1. Accessed on 23 Jan 2018

ESA (2018b) Level-1 GRD Products. https://sentinel.esa.int/web/sentinel/technical-guides/sentinel-1-sar/products-algorithms/level-1-algorithms/ground-range-detected. Accessed on 23 Jan 2018

ESA (2018c) Sentinel-2 mission details. https://earth.esa.int/web/guest/missions/esa-operational-eo-missions/sentinel-2. Accessed on 23 Jan 2018

ESA (2018d) Multispectral instrument (MSI) overview. https://earth.esa.int/web/sentinel/technical-guides/sentinel-2-msi/msi-instrument. Accessed on 23 Jan 2018

Frost VS, Stiles JA, Shanmugan KS, Holtzman JC (1982) A model for radar images and its application to adaptive digital filtering of multiplicative noise. IEEE Trans Pattern Anal Mach Intell 4(2):157–166

Giustarini L, Hostache R, Matgen P, Schumann GJP (2013) A change detection approach to flood mapping in urban areas using TerraSAR-X. IEEE Trans Geosci Remote Sens 51(4):2417–2430. https://doi.org/10.1109/TGRS.2012.2210901

GSI and NRSC (2012) Geomorphology and Lineament NGLM, Landform, 50K, Uttar Pradesh. http://bhuvan.nrsc.gov.in/gis/thematic/index.php. Accessed on 01 Jan 2012

Hirose K, Maruyama Y, Quy D-V, Tsukada M, Shiokawa Y (2001) Visualization of flood monitoring in the lower reaches of the Mekong River. Proceedings of 22nd Asian Conference on Remote Sensing, vol 1, Nov. 5–9 2001, Singapore, pp 314–319

Horritt S (1999) A statistical active contour model for SAR image segmentation. Image Vis Comput 17(3–4):213–224. https://doi.org/10.1016/S0262-8856(98)00101-2

Huang SQ (2008) Change mechanism analysis and integration change detection method on SAR images. The international archives of the photogrammetry, remote sensing and spatial information Sciences. 37(B7). Beijing

IMD (2017) Weekly weather report. http://www.imd.gov.in/pages/weeklyweatherreport.php. Accessed on 10 Sept 2017

Irrigation & Water Resource Department (2017) Flood bulletin for the year 2017. Irrigation & Water Resource Department, U.P. http://idup.gov.in/pages/en/topmenu/dept.-activities/civil/floods/en-flood-bulletin. Accessed on 10 Sept 2017

Islam MM, Sado K (2000) Development of flood hazard maps of Bangladesh using NOAA-AVHRR images with GIS. Hydrol Sci J 45:337–355. https://doi.org/10.1080/02626660009492334

Jain SK, Saraf AK, Goswami A, Ahmad T (2006) Flood inundation mapping using NOAA AVHRR data. Water Res Manage 20:949–959. https://doi.org/10.1007/s11269-006-9016-4

Jensen JR (2018) Introductory digital image processing: a remote sensing perspective, 4th edn. Pearson India Education Services Pvt. Ltd, Noida

Kass M, Witkin A, Terzopoulos D (1988) Snakes: active contour models. Int J Comput Vis 1 (4):321–331

Kumar R (2010) Fluvial processes in lower Rapti River basin: a case study of impacts on arable land. Unpublished Ph.D thesis. Centre for the Study of Regional Development, Jawaharlal Nehru University, New Delhi

Kumar R (2016) Flood hazard assessment of 2014 floods in Sonawari sub-district of Bandipore district (Jammu and Kashmir): an application of geoinformatics. Remote Sens Appl Soc Environ 4:188–203

Kumar R, Acharya P (2016) Flood hazard and risk assessment of 2014 floods in Kashmir Valley: a space-based multisensor approach. Nat Hazards 84(1):437–464

Kumar R, Kamal V, Singh RK (2013) Geomorphic effects of 2011 floods on channel belt parameters of Rapti River: a remote sensing and GIS approach. Corona J Sci Technol 2(2):4–12

Kumar R, Kumar S, Pandey PC (2016) Delineation and zonation of flood prone area using geo-hydrological parameters: a case study of lower Ghaghara River Valley. In: Srivastava PK, Pandey PC, Kumar P, Raghubanshi AS, Han D (eds) Geospatial technology for water resource applications. CRC Press, Taylor & Francis Group, Boca Raton, pp 78–100

Lee J-S (1981) Speckle analysis and smoothing of synthetic aperature radar images. Comput Graphics Image Process 17(1):24–32

Lee J-S, Jurkevich I, Dewaele P, Wambacq P, Oosterlinck A (1994) Speckle filtering of synthetic aperture radar images: a review. Remote Sens Rev 8:313–340. https://doi.org/10.1080/02757259409532206

Li J, Chen W, Touzi R (2007) Optimum RADARSAT-1 configurations for wetlands discrimination: a case study of the Mer Bleue peat bog. Can J Remote Sens 33(Suppl 1):S46–S55. https://doi.org/10.5589/m07-046

Lopès A, Nezry E, Touzi R and Laur H (1990) Maximum aposteriori speckle filtering and first order texture models in SAR Images. Proceedings International Geoscience and Remote Sensing Symposium (IGARSS'90). Ref IEEE90CH2825–8. Washington DC, USA, pp 2409–2412

Manavalan R (2017) SAR image analysis techniques for flood area mapping-literature survey. Earth Sci Inf 10(1):1–14. https://doi.org/10.1007/s12145-016-0274-2

Manavalan, Rao (2014) DEM and SAR image based flood feature extraction techniques to map the deep and shallow flood inundated regions of known as well as remote disaster regions. Geocarto Int 29(7):745–757. https://doi.org/10.1080/10106049.2013.838310

Manjusree R, Kumar LP, Bhatt CM, Rao GS, Bhanumurthy V (2012) Optimization of threshold ranges for rapid flood inundation mapping by evaluating backscatter profiles of high incidence angle SAR images. Int J Disaster Risk Sci 3(2):113–122. https://doi.org/10.1007/s13753-012-0011-5

Manjusree P, Bhatt CM, Begum A, Rao GS, Bhanumurthy V (2015) A decadal historical satellite data nalysis for flood hazard evaluation: a case study of Bihar (North India). Singap J Trop Geogr 36:308–323

Mason DC, Schumann GJP, Neal JC, Garcia-Pintado J, Bates PD (2012a) Automatic near real-time selection of flood water levels from high resolution Synthetic Aperture Radar images for assimilation into hydraulic models: a case study. Remote Sens Environ 124:705–716

Mason DC, Davenport IJ, Neal JC, Schumann GJP, Bates PD (2012b) Near real-time flood detection in Urban and rural areas using high-resolution synthetic aperture radar images. IEEE Trans Geosci Remote Sens 50(8):3041–3052

McFeeters SK (1996) The use of the normalized difference water index (NDWI) in the delineation of open water features. Int J Remote Sens 17:1425–1432

Mizushima Laboratory (2013) India Place Finder: http://india.csis.u-tokyo.ac.jp/, Department of Oriental History, Graduate School of Humanities and Sociology, The University of Tokyo

Motulsky H (2014) Intuitive biostatistics: a nonmathematical guide to statistical thinking, 3rd edn. Oxford University Press, New York

Oberstadler R, Hoè Nsch H, Huth D (1997) Assessment of the mapping capabilities of ERS-1 SAR data for flood mapping: a case study in Germany. Hydrol Process 11:1415–1425. https://doi.org/10.1002/(SICI)1099-1085(199708)11:10<1415::AID-HYP532>3.0.CO;2-2

Planning Commission (2011) Report of working group on food management and region specific issues for XII plan. Govt of India, New Delhi

Pulvirenti L, Pierdicca N, Guerriero L (2013) Monitoring flood evolution in vegetated areas using COSMO-skyMed data: the Tuscany 2009 case study. IEEE J Sel Top Appl Earth Observ Remote Sens 6(4):1939–1404

Pulvirenti L, Chini M, Pierdicca N, Boni G (2016) Use of SAR for detecting floodwater in urban and agricultural areas: the role of the interferometric coherence. IEEE Trans Geosci Remote Sens 54(3):1532–1544. https://doi.org/10.1109/TGRS.2015.2482001

Qui F, Berglund J, Jensen JR, Thakkar P, Ren D (2004) Speckle noise reduction in SAR imagery using a local adaptive filter. GISci Remote Sens 41(3):244–266

Rana NK, Kumar R, Kumar D (2009) Nature of channel shift of a foothill-fed river in the alluvial setting: a case study of River Rapti, India. Indian J Geomorphol 13(1&2):83–98

Romshoo SA, Sadaff A, Rashid I, Dar RA (2018) Climatic, geomorphic and anthropogenic drivers of the 2014 extreme flooding in the Jhelum basin of Kashmir, India. Geomat Nat Haz Risk 9 (1):224–248. https://doi.org/10.1080/19475705.2017.1417332

Sanyal J, LU X (2006) GIS-based flood hazard mapping at different administrative scales: a case study in Gangetic West Bengal, India. Singap J Trop Geogr 27:207–220. https://doi.org/10.1111/j.1467-9493.2006.00254.x

Schlaffer S, Matgen P, Hollaus M, Wagner W (2015) Flood detection from multi-temporal SAR data using harmonic analysis and change detection. Int J Appl Earth Obs Geoinf 38:15–24. https://doi.org/10.1016/j.jag.2014.12.001

Senthilnath J, Shenoy HV, Rajendra R, Omkar SN, Mani V, Diwakar PG (2013) Integration of speckle de-noising and image segmentation using Synthetic Aperature Radar image for flood extent extraction. J Earth Syst Sci 122(3):559–572. https://doi.org/10.1007/s12040-013-0305-z

Sheng Y, Xia Z (1996) A comprehensive evaluation of filters for radar speckle suppression. Proceed IGARSS 2:1559–1561

Singh IB (1996) Geological evolution of Ganga plain: an overview. J Palaeontol Soc India 41:99–137

Sivasami KS (2002) Environmental effect due to floods and reservoirs. In: Subramanian V (ed) Environmental hazard in South Asia. Capital, New Delhi, pp 65–82

Song Y-S, Sohn H-G, Park C-H (2007) Efficient water area classification using RADARSAT-1 SAR Imagery in a high relief mountainous environment. Photogramm Eng Remote Sens 73 (3):285–296

Tan Q, Bi S, Hu J, Liu Z (2004) Measuring lake water level using multisource remote sensing images combined with hydrological statistical data. IEEE Geoscience and Remote Sensing Symposium, IGARSS-2004, 7, 4885–4888. Anchorage, AK, Sept. 20–24, 2004. https://doi.org/10.1109/IGARSS.2004.1370258

Twele A, Cao WX, Plank S, Martinis S (2016) Sentinel-1-based flood mapping: a fully automated processing chain. Int J Remote Sens 37(13):2990–3004. https://doi.org/10.1080/01431161.2016.1192304

Williams DJ, Shah M (1992) A fast algorithm for active contours and curvature estimation. CVGIP: Image Underst 55(1):14–26

Xu H (2006) Modification of normalised difference water index (NDWI) to enhance open water features in remotely sensed imagery. Int J Remote Sens 27:3025–3033. https://doi.org/10.1080/01431160600589179

Yadav RP (1999) Floods in eastern U.P. Radha Publication, New Delhi-2

Yamada Y (2001) Detection of Flood-inundated area and relation between the area and Micro-Geomorphology using SAR and GIS. IEEE Geoscience and Remote Sensing Symposium, IGARSS. 7: 3282–3284. Sydney, NSW, July 9–13, 200. https://doi.org/10.1109/IGARSS.2001.978329